RSC Advances

PAPER

View Article Online
View Journal | View Issue



Cite this: *RSC Adv.*, 2020, **10**, 2932

# Hydrothermal synthesis of nitrogen-doped ordered mesoporous carbon *via* lysine-assisted self-assembly for efficient $CO_2$ capture†

Xia Wan,[ab] Yuchen Li,[ab] Huining Xiao,[*c] Yuanfeng Pan[d] and Jie Liu[ab]

Nitrogen-doped ordered mesoporous carbons (NOMCs) were synthesized by single-step hydrothermal self-assembly using F127 as a soft template, hexamine as a formaldehyde source, L-lysine as a polymerization catalyst, and 3-aminophenol as both carbon and nitrogen sources. The microstructure of the NOMCs was characterized by XRD, $N_2$ adsorption/desorption, TEM, FTIR, and XPS. The results indicated that the obtained NOMCs exhibited a large specific surface area, uniform pore size distribution and highly ordered 2-D hexagonal mesostructure (*P6mm*). Besides, the nitrogen was uniformly doped into the carbon framework in the form of various nitrogen species. The adsorption isotherms of $CO_2$ and $N_2$ were also determined and could be well fitted by a DSL model. The capture capacity of $CO_2$ was affected by both the nitrogen content and mesostructure of the adsorbents. Overall, NOMC-L-0.5 displayed excellent $CO_2$ capture capacity (0 °C, 3.32 mmol $g^{-1}$; 25 °C, 2.50 mmol $g^{-1}$), and still demonstrated great regenerability with only 2% loss after several $CO_2$ adsorption/desorption cycles. Moreover, the $CO_2/N_2$ selectivity calculated by IAST was as high as 43.2 at 25 °C in a typical composition of flue gas (binary mixtures with 15% $CO_2$). The superior adsorption performance enables NOMCs to be a promising $CO_2$ adsorbent in practical applications.

Received 28th November 2019
Accepted 6th January 2020

DOI: 10.1039/c9ra09983b

rsc.li/rsc-advances



## 1. Introduction

Increased global atmospheric $CO_2$ concentration caused by fossil fuel combustion is the main cause of global climate deterioration, and the value of which reached 401 ppm in 2013, an increase of 42.8% compared with the pre-industrial period, and it is predicted to reach 800 ppm by 2100.[1,2] In order to reduce the harm caused by excessive $CO_2$ emissions, the development of $CO_2$ capture technologies is of particular importance. Among current $CO_2$ capture technologies, adsorption of $CO_2$ through porous solid adsorbents has been promoted significantly due to its environmentally friendly and economic advantages over conventional chemical absorption using aqueous amine solutions.[3,4] A large number of porous adsorbents have been studied, including metal–organic frameworks (MOFs),[5] zeolites,[6] ordered mesoporous silica,[7] polymers[8] and porous carbons.[9,10] Among them, porous carbons such as activated carbons,[11] carbon nanofibers,[12,13] and carbon nanotubes,[14,15] show the promise as $CO_2$ adsorbents owing to the high surface area, large porosity, outstanding stability under various conditions, low regeneration energy costs, and extensive in raw material source.[16] Numerous reports have shown that the $CO_2$ capture capacity and selectivity of porous carbons will be significantly improved after the introduction of nitrogen functional groups into carbon framework.[17,18] Sethia *et al.*[19] synthesized high-nitrogen-content activated carbons which displayed superior $CO_2$ capture capacity of 5.4 mmol $g^{-1}$ at 25 °C and 100 kPa. Pevida *et al.*[20] prepared nitrogen-doped mesoporous carbon through the use of melamine as nitrogen source, presenting a high capture capacity for $CO_2$ (2.25 mmol $g^{-1}$, 25 °C, 100 kPa).

Generally, there are two main approaches to incorporate nitrogen: (1) direct synthesis of nitrogen-containing precursors,[21,22] (2) modified with nitrogen-containing groups after carbon synthesis.[23] The direct method is even better owing to the controllable chemical composition and uniform nitrogen distribution.[24,25] There are several direct routes in the synthesis of nitrogen-containing precursors to obtain nitrogen-doped highly ordered mesoporous carbon.

The hard-template method for preparing nitrogen-doped mesoporous carbon requires the polymerization of carbon precursors and nitrogen sources in the pores of the hard template. This method has the advantages of adjustable pore channels but requires a template removal afterwards, which is

[a]*Hebei Key Lab of Power Plant Flue Gas Multi-Pollutants Control, North China Electric Power University, Baoding, 071003, P. R. China*

[b]*School of Environmental Science and Engineering, North China Electric Power University, Baoding, 071003, P. R. China*

[c]*Department of Chemical Engineering, University of New Brunswick, Fredericton, New Brunswick E3B 5A3, Canada. E-mail: hxiao@unb.ca*

[d]*School of Chemistry and Chemical Engineering, Guangxi University, Nanning, 530004, P. R. China*

† Electronic supplementary information (ESI) available. See DOI: 10.1039/c9ra09983b

time-consuming, complicated, and poorly industrially applicable.[26,27] Compared with hard-template method, the evaporation induced self-assembly (EISA) method has great advantages of synthesizing nitrogen-doped ordered mesoporous carbon with different structures and properties.[28,29] However, EISA method demonstrates some shortcomings, such as the need for large-scale coating, multiple steps and the consumption of large amounts of organic solvents that are difficult to recycle, indicating the difficulties in large-scale industrial application.[30]

To overcome these limitations, the approach of hydrothermal cooperative self-assembly was selected to prepare nitrogen-doped ordered mesoporous carbon. The approach is usually a collaborative self-assembly process between soft templates (*i.e.* Pluronic F127) and phenol formaldehyde resol.[31,32] The key to obtain carbon materials with excellent mesostructure *via* this method is to control the reaction rate of phenolic polymerization. It is worth noting that previous studies indicated that amino acids can be involved in the assembly of polymers and promote the formation of mesostructures.[33,34]

In this work, the nitrogen-doped ordered mesoporous carbons (NOMCs) were synthesized by a simple one-step hydrothermal self-assembly with the use of Pluronic F127 as soft template, resorcinol as carbon source, 3-aminophenol as both carbon and nitrogen sources, L-lysine as polymerization catalyst, mesostructure assembly promoter and nitrogen source. It is worth mentioning that hexamethylenetetramine (HMT) was used as a slow release source of formaldehyde, which could be hydrolyzed to form formaldehyde and ammonia slowly at an elevated temperature, thus controlling the reaction rate of phenolic polymerization well, together with the assist of L-lysine. As a result, there is no need for additional pre-polymerization steps.[35] Moreover, the physicochemical properties of the NOMCs were analyzed by various characterization methods; and the $CO_2$ adsorption performance was also determined.

# 2. Experimental

## 2.1. Materials

Triblock poly(ethylene oxide)-*b*-poly(propylene oxide)-*b*-poly(-ethylene oxide) copolymer Pluronic F127 ($M_w$ = 12 600, $PEO_{106}PPO_{70}PEO_{106}$) was purchased from Sigma-Aldrich. Hexamethylenetetramine (HMT), L-lysine, resorcinol and 3-aminophenol were purchased from Aladdin. All chemicals were used as received without further purification. Deionized water was used in all experiments.

## 2.2. Synthesis of adsorbents

The nitrogen-doped ordered mesoporous carbon samples (NOMCs) were synthesized following the one-step hydrothermal self-assembly route. In a typical synthesis, 2.2 g of Pluronic F127, 0.292 g of L-lysine, and known amounts of phenols were added to 36 ml of deionized water and stirred at room temperature for 30 min. Then 0.7 g of HMT was added. After stirred for another 1 h, the mixture was transferred into a hydrothermal reactor with Teflon liner, and further crystallized at 100 °C for 24 h. The obtained polymer was separated by filtered and washed with deionized water for three times, followed by drying at 60 °C for 12 h in an oven. The yield of product based on phenolic resin is about 62%. Finally, the product was calcined under $N_2$ atmosphere at 350 °C for 3 h and then at 800 °C for 3 h with a heating rate of 1 °C $min^{-1}$.

During the synthesis, the total amount of phenols (resorcinol and nitrogen-rich phenol derivative: 3-aminophenol) was fixed at 0.01 mol. And the mole fraction of 3-aminophenol in total phenolic compound of the prepared nitrogen-doped ordered mesoporous carbons were 0, 50%, and 100%. Accordingly, the carbon samples were named as NOMC-L, NOMC-L-0.5, and NOMC-L-1, respectively.

## 2.3. Characterization

The low angle X-ray diffraction (XRD) patterns were recorded on a LabX-6000 X-ray diffract meter (Shimadzu, Japan) with Cu/K$\alpha$ radiation ($\lambda$ = 0.154056 nm) operating at 40 kV and 50 mA. $N_2$ adsorption/desorption isotherms were obtained by a SA 3100 surface area and pore size analyzer (Beckman Coulter, U.S.A) at 77 K. Before the measurements, each sample was pretreated under vacuum at 120 °C for 10 h. The specific surface area was calculated by using Brunauer–Emmett–Teller (BET) method at a relative pressure ($P_S/P_0$) range of 0.05–0.2. The pore size distribution was obtained from the desorption branch of isotherm through the Barrett–Joyner–Halenda (BJH) model. And the total pore volume was determined on the basis of the volume of liquid nitrogen adsorbed at $P_S/P_0$ = 0.98. The morphology was determined by a Tecnai $G^2$ F30 transmission electron microscope (TEM, FEI, U.S.A). The surface functionalities were performed on a Tensor II Fourier transform infrared (FTIR) spectrometer (Bruker Optics, German) at a resolution of 4 $cm^{-1}$ over the wave number range of 400–4000 $cm^{-1}$. The surface chemical species was examined on a ESCALAB 250Xi X-ray photoelectron spectroscope (XPS, Thermo Fisher Scientific, U.S.A) with Al/K$\alpha$ radiation ($h\nu$ = 1486.6 eV).

## 2.4. Isothermal adsorption measurements

Pure component ($CO_2$ and $N_2$) adsorption isotherms were tested on a JW-BK122W static adsorption analyzer (JWGB Sci & Tech Co. Ltd, China) at different temperatures (0 °C, 25 °C) under pressure range of 0 to 100 kPa for the NOMCs. During the measurement, helium (99.999%), nitrogen (99.999%) and carbon dioxide (99.999%) with ultra-high purity were used. Each sample was degassed under vacuum at 120 °C for 10 h prior to the adsorption isotherms measurements. In order to evaluate the regenerability of the adsorbent, the adsorption was conducted at 25 °C up to 100 kPa and the desorption was performed at 25 °C under vacuum. The $CO_2$ adsorption/desorption process was carried out repeatedly by multiple times in the same manner to test the cyclic adsorption stability.

# 3. Results and discussion

## 3.1. Characteristics of NOMCs

**3.1.1. Textural and structural properties of NOMCs.** The structural information of NOMCs was obtained by small-angle

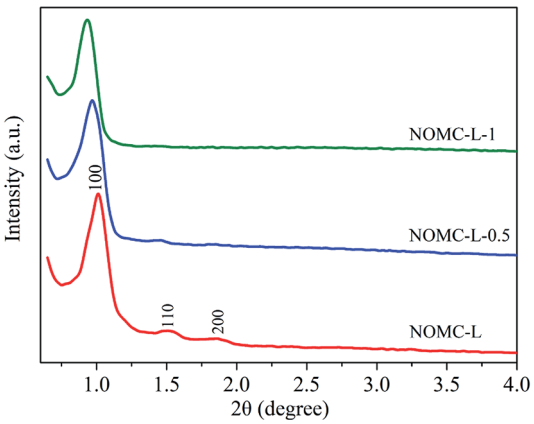


Fig. 1 Small-angle XRD patterns of NOMCs.

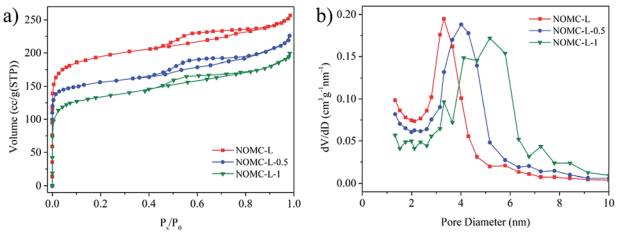


Fig. 2 $N_2$ adsorption/desorption isotherms (a) and pore size distribution curves (b) of NOMCs.

XRD diffraction shown in Fig. 1. Basically, XRD patterns of all the carbon samples reveal well-resolved peaks at 0.5–2.5° of $2\theta$. NOMC-L presents three strong diffraction peaks with a $d$-spacing ratio of $1/(1/\sqrt{3})/(1/2)$, which can be indexed as (100), (110), and (200) reflections, implying an excellent textural uniformity and highly ordered mesostructure of two-dimensional (2-D) hexagonal symmetry (space group *P6mm*).[36,37] With the increase amount of 3-aminophenol, the intensity of the diffraction peaks became weakened, NOMC-L-0.5 still preserves the three characteristic XRD peaks, while NOMC-L-1 with 3-aminophenol used alone shows only one visible (100) reflection, which indicated that the regularity of mesostructure progressively reduced with the increment of 3-aminophenol dosage during the synthesis of carbon samples.

The textural properties of the NOMCs were obtained by $N_2$ adsorption/desorption analysis. The corresponding structural parameters such as the specific surface area ($S_{BET}$), pore volume ($V_p$), and average pore diameter ($d_p$) are listed in Table 1. As shown in Fig. 2a, all the nitrogen-doped samples show the type IV $N_2$ adsorption/desorption isotherms with clear hysteresis loop, demonstrating typically mesoporous structure of NOMCs.[38] With the enhancement of 3-aminophenol, the $N_2$ isotherms represented a decreased adsorption capacity and a reduced hysteresis loop, indicating a downward trend of the BET specific surface area and pore volume. Besides, the pore size distribution of three NOMCs is within the mesopore range (Fig. 2b). NOMC-L exhibits a narrow pore size distribution mostly at 3.3 nm. As 3-aminophenol dosage rises, the pore size distribution becomes less concentrated and a gradually increasing pore size value is obtained. NOMC-L-0.5 can still maintain a relatively narrow pore size distribution, while the pore size distribution of NOMC-L-1 shows a wide range of 3.15 to 7.24 nm. The results indicated that excessive 3-aminophenol might reduce the orderness and uniformity of the carbon samples.

The morphology of NOMCs was observed using TEM. The images shown in Fig. 3a and b reveal a clearly highly ordered mesostructure of NOMC-L and NOMC-L-0.5, while a degradation of mesostructure can be seen in NOMC-L-1 (Fig. 3c). This phenomenon indicates that the orderness of the mesostructure of NOMCs was gradually weakened as 3-aminophenol dosage increased, which is consistent with the results of XRD diffraction and $N_2$ adsorption/desorption analysis. Moreover, the HAADF-STEM image and the corresponding elemental mapping of NOMC-L-0.5 is shown in Fig. 3d, which presents the homogeneous distribution of C, N, and O, suggesting the nitrogen was uniformly doped into the carbon framework.

**3.1.2. Surface chemical properties of NOMCs.** Fig. 4 shows the FT-IR spectra of NOMCs which revealed the surface functionalities of the samples. As can be seen from the figure, the band position of the spectra for NOMCs presented high degree of similarity. The peaks at ~3444 $cm^{-1}$ and ~1637 $cm^{-1}$ were attributed to the adsorbed water.[39,40] While the bands at ~1384 and ~1100 $cm^{-1}$ corresponded to C–N stretching vibration.[41] Besides, the intensity of the characteristic bands of nitrogen gradually became stronger with an increase in the amount of 3-aminophenol. Herein, the results of FTIR confirmed the formation of N-doped carbon frameworks, and indicated the nitrogen content of NOMCs increased with the enhancement of 3-aminophenol dosage.

The functionalities presented on the surface of NOMCs were further confirmed by means of XPS analysis. In the survey spectra (Fig. 5), three typical peaks at ~285, ~400, and ~533 eV

Table 1 Structural properties, elemental composition and $CO_2$ capture capacities of NOMCs

| Samples | $S_{BET}$ ($m^2$ $g^{-1}$) | $V_p$ ($cm^3$ $g^{-1}$) | $d_p$ (nm) | Elemental composition (at%) | | | $CO_2$ capture capacity (mmol $g^{-1}$) | |
|---|---|---|---|---|---|---|---|---|
| | | | | C | O | N | 0 °C | 25 °C |
| NOMC-L | 435 | 0.235 | 3.312 | 91.8 | 7.1 | 1.1 | 2.59 | 2.07 |
| NOMC-L-0.5 | 387 | 0.212 | 4.298 | 91.2 | 6.3 | 2.5 | 3.32 | 2.50 |
| NOMC-L-1 | 351 | 0.198 | 5.179 | 91.0 | 5.4 | 3.6 | 3.12 | 2.10 |

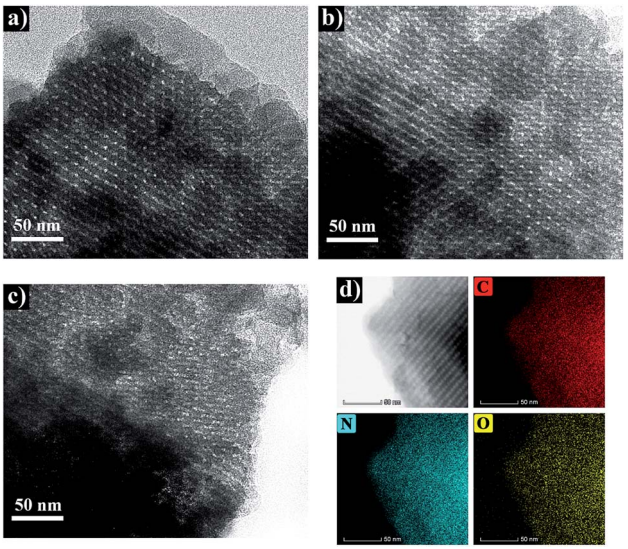


Fig. 3 TEM images of NOMC-L (a), NOMC-L-0.5 (b), and NOMC-L-1 (c); (d) HAADF-STEM image and the corresponding elemental mapping of NOMC-L-0.5.

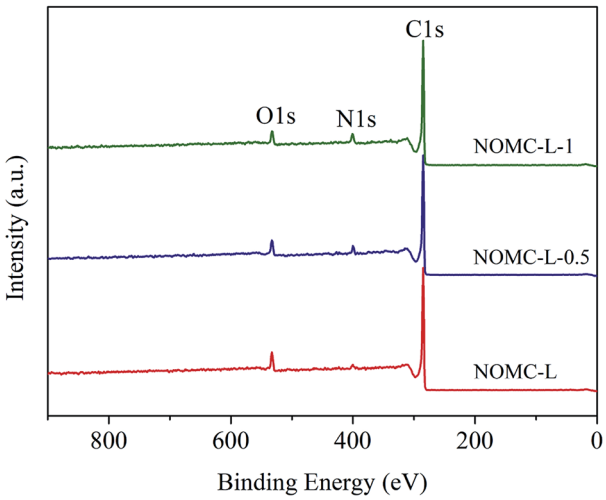


Fig. 5 XPS survey scan spectra of NOMCs.

that could be attributed to carbon (C 1s), nitrogen (N 1s), and oxygen (O 1s), and the corresponding element contents are summarized in Table 1, respectively. As can be seen, the content of nitrogen is positively related to 3-aminophenol dosage, which increased from 1.1 at% of NOMC-L to 3.6 at% of NOMC-L-1.

The nature of C, O, and N species in the NOMCs were further studied based on high-resolution XPS spectra. Fig. 6a–c show that the C 1s spectra of all three NOMCs demonstrate the presence of four peaks with different binding energies (B.E.) and concentrations (Table 2). C1 (~284.5 eV) is assigned for $sp^2$ (C=C) and $sp^3$ (C–C) carbon atoms. C2 (~285 eV) corresponds to carbon in phenol, alcohol or ether (C–O) and/or C=N bond, while C3 (~286 eV) to carbonyl or quinone groups (C=O) and/or C–N linkage, and C4 (288 eV) to carboxyl or ester linkages (O=C–O).[42] The content of C3 peak shows an increasing trend with enhancement in nitrogen content of the samples, demonstrating the successful doping of nitrogen into the carbon frameworks.

As seen in Fig. 6d–f and Table 2, the O 1s spectra of NOMCs reveal the following three peaks: O1 (~531 eV), O2 (~532.8 eV), and O3 (~533.8 eV), which are associated with carbonyl, ketone or lactone groups (C=O); alcohol, phenol or ether groups (C–O); and carboxyl group (O=C–OH).[43] As previous literature reported, the O1 and O2 peaks are related to basicity while O3 peak is in charge of acidity. Thus, the samples with addition of 3-aminophenol, *i.e.* NOMC-L-0.5 and NOMC-L-1, exhibit higher basicity in nature, which is conducive to $CO_2$ capture.

As shown in Fig. 6g–i and Table 2, the N 1s spectra exhibited four peaks with binding energies at ~389 eV, ~400 eV, ~401 eV, and ~402 eV, which were ascribed to pyridinic-N (N-6), pyrrolic-N (N-5), quaternary-N (N-Q), and oxidized-N (N-X) respectively.[44] N-6 and N-5 exhibited Lewis basic characteristics for the contribution of p-electrons to π-system, thus providing abundant adsorption sites for $CO_2$. Moreover, the proportion of N-6 and N-5 in the total N content increased from 47.13% (NOMC-L) to 54.98% (NOMC-L-0.5) and 61.41% (NOMC-L-1) after adding 3-aminophenol, which enabled the NOMCs to capture $CO_2$ effectively.

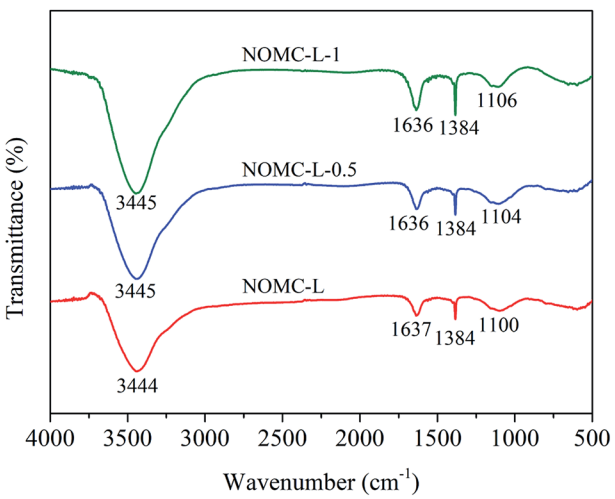


Fig. 4 FT-IR spectra of NOMCs.

### 3.2. $CO_2$ adsorption properties

**3.2.1. Adsorption equilibrium study.** The $CO_2$ and $N_2$ capture capacities of NOMCs were studied at 0 °C and 25 °C under 100 kPa, respectively, and the experimental adsorption isotherms are presented in Fig. 7. For all three carbon adsorbents, the $CO_2$ capture capacity was decreased with increasing temperature in the range of 0–100 kPa, which can be due to the increased thermal energy of $CO_2$ molecules at higher temperature, indicating an exothermic physical adsorption in the process of $CO_2$ adsorption on NOMCs. The results showed that NOMC-L-0.5 and NOMC-L-1 presents higher $CO_2$ capture capacity than NOMC-L, which proves that nitrogen doping can improve the adsorption of $CO_2$. However, NOMC-L-1 with the

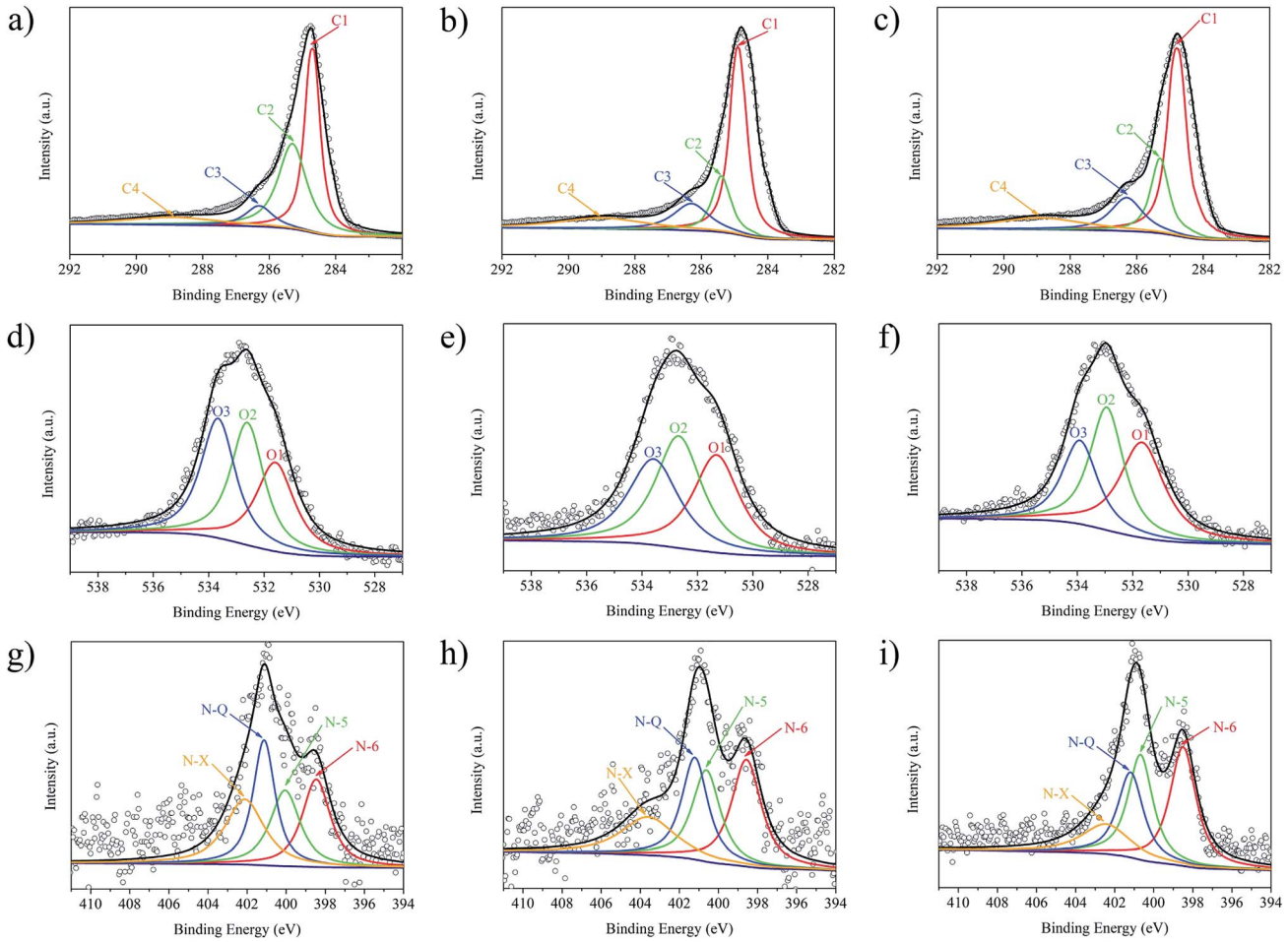


Fig. 6 Deconvoluted high-resolution C 1s (a–c), O 1s (d–f) and N 1s (g–i) XPS spectra of NOMC-L, NOMC-L-0.5, and NOMC-L-1.

highest nitrogen content exhibits a lower $CO_2$ capture capacity than NOMC-L-0.5, the result may be attributed to that, apart from the nitrogen content, the mesostructure such as the specific surface area of the samples is also an important factor influencing $CO_2$ capture performance. Apparently, under the combined influence of the above two reasons, NOMC-L-0.5 shows the maximum $CO_2$ capture capacity of 3.32 mmol $g^{-1}$ at 0 °C and 2.50 mmol $g^{-1}$ at 25 °C under 100 kPa (Table 1), which is higher than N-enriched porous carbons with urea modification.[45] Moreover, the capture capacity of $CO_2$ is much higher than that of $N_2$ in whole pressure range, showing a great separation selectivity of $CO_2$ *vs.* $N_2$.

Table 2 XPS data of C 1s, O 1s, and N 1s core level of NOMCs

| | NOMC-L | | NOMC-L-0.5 | | NOMC-L-1 | |
|---|---|---|---|---|---|---|
| Samples | B.E. | at% | B.E. | at% | B.E. | at% |
| C1 | 284.8 | 43.50 | 284.5 | 43.90 | 284.6 | 44.27 |
| C2 | 284.9 | 35.62 | 284.9 | 28.23 | 285.4 | 25.66 |
| C3 | 286.1 | 9.20 | 285.4 | 13.89 | 286.6 | 15.26 |
| C4 | 288.9 | 11.68 | 287.4 | 13.98 | 289.7 | 14.81 |
| O1 | 531.6 | 29.48 | 531.3 | 32.38 | 531.7 | 37.15 |
| O2 | 532.6 | 35.07 | 532.6 | 36.64 | 532.9 | 37.55 |
| O3 | 533.7 | 35.45 | 533.6 | 30.98 | 533.8 | 25.30 |
| N-6 | 398.5 | 24.60 | 398.5 | 30.46 | 398.5 | 33.52 |
| N-5 | 400.1 | 22.53 | 400.6 | 24.52 | 400.6 | 27.89 |
| N-Q | 401.1 | 27.43 | 401.2 | 25.38 | 401.1 | 23.34 |
| N-X | 402.1 | 25.44 | 403.6 | 19.64 | 402.4 | 15.24 |

**3.2.2. Adsorption isotherm model.** The fitting of isothermal adsorption experimental data with mathematical models contributes to a better description of adsorption behavior. In this work, the Langmuir, Freundlich, Temkin, and dual-site Langmuir (DSL) isotherm models were used to analyze the adsorption equilibrium data of pure $CO_2$ and $N_2$ on NOMCs.

The Langmuir isotherm model assumes the energetically homogeneous adsorbent surface, and there is no interaction between the adsorbed molecules, which is suitable for describing monolayer adsorption.[46] The Freundlich isotherm model assumes that the surface coverage of adsorbent is negatively correlated with the adsorption energy, leading to the description of heterogeneous adsorption.[47] The Temkin isotherm model shows the faction related to the adsorbent–adsorbate interaction, which assumes the adsorption heat of adsorbed molecules in the layer reduced linearly.[48] The DSL isotherm model is extended from the single site Langmuir model, which explicitly takes into account of the surface

 

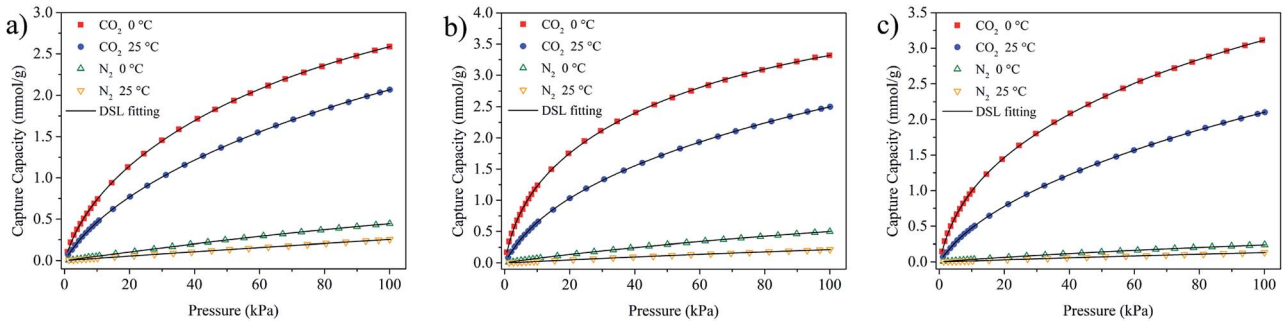


Fig. 7 $CO_2$ and $N_2$ adsorption isotherms of NOMC-L (a), NOMC-L-0.5 (b), and NOMC-L-1 (c) (points, experimental data; curves, DSL fitting model) at 0 °C and 25 °C.

heterogeneity.[49] Therefore, the assumption manifests as there are two types of adsorption sites with different characteristic energies at the adsorbent surface. The adsorption sites with strongest energy are occupied first, followed by the occupation of the weak ones.

The equations of the above isotherm models can be represented as eqn (1)–(4):

$$q = q_m \frac{k_L p}{1 + k_L p} \quad (1)$$

$$q = k_F p^{1/n} \quad (2)$$

$$q = B \ln(k_T p) \quad (3)$$

$$q = q_{m,1} \frac{b_1 p}{1 + b_1 p} + q_{m,2} \frac{b_2 p}{1 + b_2 p} \quad (4)$$

where $q$ is the equilibrium capture capacity (mmol $g^{-1}$); $p$ is the pressure (kPa); $q_m$ is the maximum capture capacity (mmol $g^{-1}$); $k_L$ is Langmuir constant ($kPa^{-1}$); $k_F$ (mmol $g^{-1}$ $kPa^{-1/n}$) and $n$ are Freundlich constants; $B$ and $k_T$ (mmol $g^{-1}$ $kPa^{-1}$) are Temkin constants; $q_{m,i}$ is the maximum capture capacity of site $i$ (mmol $g^{-1}$); $b_i$ is the affinity parameter of site $i$ ($kPa^{-1}$).

Fig. S1† shows the accuracy comparison of Langmuir, Freundlich, Temkin and DSL isotherm models fitting the experimental data of pure $CO_2$ and $N_2$ adsorption on NOMCs at 0 °C and 25 °C. And the corresponding fitting parameters of the isotherm models are listed in Tables S1, S2, S3 and S4,† respectively.

The results indicated that compared with Langmuir, Freundlich and Temkin model, DSL model showed the highest accuracy in fitting all set of experimental data of pure $CO_2$ on NOMCs at 0 °C and 25 °C, and revealed the highest correlation coefficients ($R^2$) over 0.9999. As for pure $N_2$, the experimental isotherm data were well fitted by Langmuir, Freundlich and DSL models due to the linear shape of $N_2$ adsorption isotherms.[50] Among them, the DSL model displays the highest $R^2$ value, suggesting that the adsorption behavior of $CO_2$ and $N_2$ on NOMCs can be well described by DSL model. The nearly perfect agreement of DSL model with all experimental isotherm data is exhibited in Fig. 7.

As can be seen from the values of DSL model parameters in Table S4,† the value of $q_m$ and affinity constant $b$ for $CO_2$ and $N_2$ decreases with the increment in adsorption temperature, demonstrating an exothermic property of the adsorption process.[51] Moreover, all the adsorbents reveal a higher $CO_2$ affinity over $N_2$ attributed to the higher $q_m$ and $b$ of $CO_2$ isotherm models. Among the two sites with different parameters, site 1 with larger $b$ value is regarded as strong free energy site for the adsorption of $CO_2$ and $N_2$, while the weak free energy site is site 2, indicating an energetical heterogeneity surface of the NOMCs.

**3.2.3. Isosteric heat of adsorption.** The isosteric heat of adsorption ($Q_{st}$) is a thermodynamic assessment of the interaction between adsorbent and adsorbate, and also is a significant parameter for evaluating the uniformity of adsorbent surface. The $Q_{st}$ is usually calculated by adsorption isotherms of $CO_2$ at different temperatures through the Clausius–Clapeyron equation presented in eqn (5).[52]

$$Q_{st} = \frac{RT_1T_2 \ln(p_2/p_1)}{T_2 - T_1} \quad (5)$$

where $Q_{st}$ is the isosteric heats of adsorption (kJ $mol^{-1}$); $T$ is the adsorption temperature (K); $R$ is the gas constant (8.314 J $K^{-1}$ $mol^{-1}$); $p_i$ is the equilibrium pressure at $T_i$ (kPa), which was determined from the corresponding adsorption isotherm fitted by DSL model at a given $CO_2$ capture capacity (0.25–2.0 mmol $g^{-1}$).

As shown in Fig. 8, the value of $Q_{st}$ for NOMCs displays a downward trend with the increasing capture capacity of $CO_2$, which is attributed to the surface heterogeneity. During the adsorption process, $CO_2$ molecules preferentially adsorb on the active adsorption sites, *i.e.* the basic nitrogen sites of NOMCs, resulting in a high initial $Q_{st}$; as the $CO_2$ loading increases, the high-energy sites have been saturated, $CO_2$ can only react with the weaker sites, resulting in the weakening of adsorbate–adsorbent interaction and the reduction of $Q_{st}$ value. Besides, the initial $Q_{st}$ at low $CO_2$ loading (0.25 mmol $g^{-1}$) of NOMCs is in the range of 18.2 to 30.3 kJ $mol^{-1}$, which is similar to the values reported for other nitrogen-doped carbon adsorbents and much lower than the energy required to cut the $CO_2$ chemical bonds (749 kJ $mol^{-1}$),[53,54] indicating that physical adsorption is the main process between $CO_2$ and NOMCs. Notedly, with the increasing nitrogen content of NOMCs, the initial $Q_{st}$ increased gradually, and NOMC-L-1 shows the highest

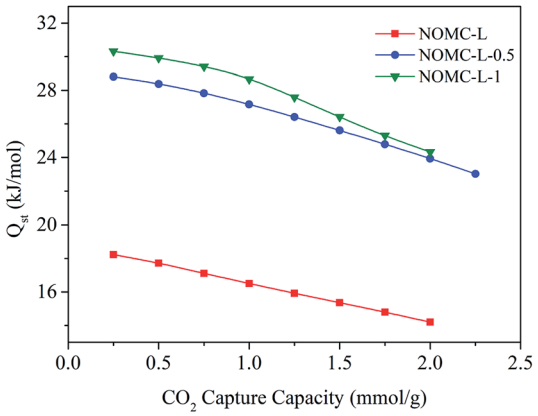


Fig. 8 Isosteric heat of $CO_2$ adsorption for NOMCs.

$Q_{st}$ value. The probable reason is that the nitrogen doping process provides strong binding sites for $CO_2$ adsorption, which enhances the interaction between adsorbents and $CO_2$ molecule, and also demonstrates the significance of nitrogen-containing groups in $CO_2$ absorption.[55] Moreover, a higher $Q_{st}$ value indicates a stronger interaction between $CO_2$ and adsorbent, which is conducive to $CO_2$ capture, while a lower $Q_{st}$ facilitates regeneration of the adsorbent. Therefore, the moderate $Q_{st}$ value of NOMCs with moderate $Q_{st}$ will be propitious to the practical application.

**3.2.4. Adsorption selectivity.** In addition to a good capture capability, a high selectivity is also an important property for the application of highly efficient adsorbents in the field of $CO_2$ capture. The adsorbent with high selectivity allows the $CO_2$ component in the mixed gas to be almost completely captured, with little interference from other coexisting gases during adsorption, facilitating subsequent storage and reuse. However, from a practical perspective, the adsorption experimental data of mixed gases cannot be collected easily and rapidly. Fortunately, the ideal adsorbed solution theory (IAST) proposes an effective method for predicting the adsorption selectivity of mixed gas from the pure component isotherms, which was first proposed by Myers and Prausnitz and has been widely and successfully used for gas adsorption of various adsorbents due to its accuracy.[56] The basic assumption of the IAST is that the adsorbed solution is ideal under constant spreading pressure and temperature, the adsorption equilibrium is considered between adsorbed phase and gas phase, and all components in the adsorbed phase presents unity activation coefficients.[57–59] Briefly, IAST theory is analogous to Raoult's law for vapor–liquid equilibrium, and the basic equation is shown in eqn (6):

$$py_i = p_i^0(\pi)x_i \tag{6}$$

where $x_i$ and $y_i$ are the mole fraction in the adsorbed phase and gas phase; $p$ and $p_i^0(\pi)$ are the equilibrium gas phase pressure for sorption of the mixture and pure component $i$ respectively, under the same spreading pressure, $\pi$. The spreading pressure is given by the Gibbs adsorption isotherm as eqn (7):

$$\frac{\pi A}{RT} = \int_0^{p_i^0} \frac{q_i(p)}{p}\mathrm{d}p \tag{7}$$

where $A$ is the specific surface area of the adsorbent; $R$ is the gas constant (8.314 J $K^{-1}$ $mol^{-1}$); $T$ is the temperature (K); and $q_i$ is the adsorption isotherm model in terms of pressure $p$ for pure component $i$.

At a constant temperature, $\pi$ is identical for all the components in the mixture, the IAST requires

$$\int_0^{p_i^0} \frac{q_i(p)}{p}\mathrm{d}p = \int_0^{p_j^0} \frac{q_j(p)}{p}\mathrm{d}p \tag{8}$$

The restraint condition for the mole fraction in adsorbed phase and gas phase of all components in mixture are presented as eqn (9):

$$\sum_i x_i = \sum_i y_i = 1 \tag{9}$$

Adsorption selectivity of component $i$ over component $j$ in the mixture $S_{ij}$ is defined by eqn (10):

$$S_{i/j} = \frac{x_i/x_j}{y_i/y_j} \tag{10}$$

For the accuracy of the selectivity of multi-component systems predicted by IAST theory, it is necessary to use an isothermal adsorption model that can precisely fit the pure component adsorption data. As previously known, the DSL model can successfully fit the experimental data of $CO_2$ and $N_2$ adsorption for full range of pressure (0–100 kPa). Thus, with the combination of DSL model and IAST, the $CO_2/N_2$ adsorption selectivity on NOMCs was calculated for the mixed gas including $CO_2$ and $N_2$, which is the main binary system in the flue gas of thermal power plants, at 25 °C with 15% $CO_2$ (typical composition of flue gas), and the corresponding results are presented in Fig. 9.

The results indicate that the selectivities of $CO_2/N_2$ on three NOMCs displayed a growing trend with the increase of pressure. The situation could be the result of a stronger interaction of NOMCs with $CO_2$ than that of $N_2$. As pressure increases, the capture capacity of $CO_2$ on the sample is significantly enhanced, while the increment of $N_2$ does not change obviously, leading to an increasing $CO_2/N_2$ selectivity. Moreover, the samples with high nitrogen content can significantly improve the selectivity of $CO_2/N_2$. For instance, at 25 °C and 100 kPa, the $CO_2/N_2$ selectivity of NOMC-L-0.5 and NOMC-L-1 reached up to 43.2 and 52.7 respectively, which is 34% and 64% higher than that of NOMC-L. Such high $CO_2/N_2$ selectivity is better than or comparable with those achieved by the nitrogen-enriched microporous carbonaceous sorbents produced by biomass carbonization and chemical activation,[60–62] though NOMCs have relatively low $CO_2$ capture capacities.

The highest selectivity appears in NOMC-L-1, however, the capture capacity of $CO_2$ on NOMC-L-0.5 with submaximal selectivity was superior, which is suggested that in order to obtain

 

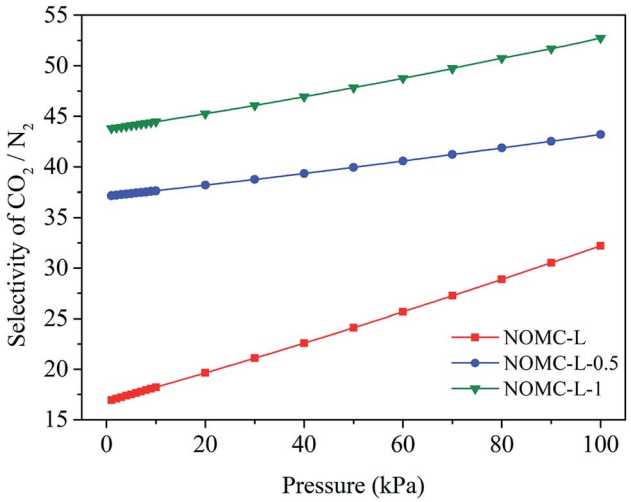


Fig. 9 IAST-predicted selectivity for $CO_2/N_2$ (15 : 85) binary mixtures on NOMCs at 25 °C.

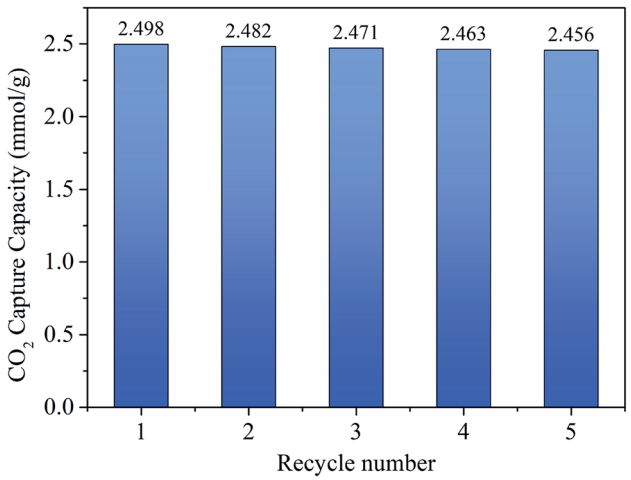


Fig. 10 $CO_2$ adsorption/desorption cycles for NOMC-L-0.5 at 25 °C.

a sample with both high selectivity and large $CO_2$ capture capacity, it may be necessary to balance the relationship between the nitrogen content and the mesostructure of samples.

**3.2.5. Cyclic adsorption performance.** Regenerability and stability are critical factors in assessing the potential industrial applications of adsorbent. Five cycles of $CO_2$ adsorption/desorption test on the absorbent NOMC-L-0.5 were conducted at 25 °C. As shown in Fig. 10, the capture capacity of $CO_2$ displays no obvious decrease after five consecutive cycles, and the desorption efficiency of $CO_2$ remains as high as 98%. The results indicated that the $CO_2$ adsorption is reversible and NOMC-L-0.5 exhibits highly stable and recyclable nature, suggesting a great feasibility in practical applications of $CO_2$ capture.

## 4. Conclusions

In summary, a series of nitrogen-doped ordered mesoporous carbons (NOMCs) were successfully prepared without prepolymerization through a single-step hydrothermal self-assembly in the presence of Pluronic F127 as soft template and basic L-lysine as polymerization catalyst and mesostructure assembly promoter. In addition to the partial nitrogen provided by L-lysine, it is possible to introduce more nitrogen while selecting the high-nitrogen-content 3-aminophenol as carbon source. The results showed NOMCs exhibited large surface area, uniform pore size, highly ordered mesostructure (*P6mm*), and high surface nitrogen content (1.1–3.6 at%). As 3-aminophenol dosage rose, the nitrogen content of NOMCs gradually increased, whereas excessive 3-aminophenol could lead to the degradation of mesostructure. NOMC-L-0.5 with moderate nitrogen content displayed the highest $CO_2$ capture capacity (3.32 mmol $g^{-1}$ at 0 °C and 2.50 mmol $g^{-1}$ at 25 °C at 100 kPa), which can be ascribed to the fact that both nitrogen content and mesostructure played essential roles in excellent $CO_2$ adsorption performance under discussed condition. The DSL model was used to predict pure component isotherm data in the tested temperature and pressure ranges and exhibited considerable accuracy. In addition, IAST-predicted $CO_2$ selectivity over $N_2$ of NOMC-L-0.5 showed a high value of 43.2 for $CO_2/N_2$ mixtures (15 : 85, similar to flue gas composition) at 25 °C and 100 kPa. The adsorbent also exhibits excellent regenerability and stability in the cyclic $CO_2$ adsorption/desorption test. Overall, the proposed NOMC-L-0.5 can be regarded as an efficiently potential adsorbent for the application of $CO_2$ removal industry.

## Conflicts of interest

There are no conflicts to declare.

## Acknowledgements

This work was supported by NSERC Canada and Fundamental Research Funds for the Central Universities (2019MS108).

## References

1 F. A. A. Kareem, A. M. Shariff, S. Ullah, F. Dreisbach, L. K. Keong, N. Mellon and S. Garg, Experimental measurements and modeling of supercritical $CO_2$ adsorption on 13X and 5A zeolites, *J. Nat. Gas Sci. Eng.*, 2018, **50**, 115–127.
2 V. Scott, S. Gilfillan, N. Markusson, H. Chalmers and R. S. Haszeldine, Last chance for carbon capture and storage, *Nat. Clim. Change*, 2013, **3**, 105–111.
3 Z. Tian, Y. Qiu, J. Zhou, X. Zhao and J. Cai, The direct carbonization of algae biomass to hierarchical porous carbons and $CO_2$ adsorption properties, *Mater. Lett.*, 2016, **180**, 162–165.
4 D. M. D'Alessandro, B. Smit and J. R. Long, Carbon dioxide capture: prospects for new materials, *Angew. Chem., Int. Ed.*, 2010, **49**(35), 6058–6082.
5 M. Montazerolghaem, S. F. Aghamiri, S. Tangestaninejad and M. R. Talaiea, A metal–organic framework MIL-101 doped with metal nanoparticles (Ni & Cu) and its effect on $CO_2$ adsorption properties, *RSC Adv.*, 2016, **6**(1), 632–640.

6 J. Zhou, W. Li, Z. Zhang, W. Xing and S. Zhuo, Carbon dioxide adsorption performance of N-doped zeolite Y templated carbons, *RSC Adv.*, 2012, **2**(1), 161–167.

7 P. López-Aranguren, S. Builes, J. Fraile, A. López-Periago, L. F. Vega and C. Domingo, Hybrid aminopolymer–silica materials for efficient $CO_2$ adsorption, *RSC Adv.*, 2015, **5**(127), 104943–104953.

8 R. Bera, M. Ansari, S. Mondal and N. Das, Selective $CO_2$ capture and versatile dye adsorption using a microporous polymer with triptycene and 1,2,3-triazole motifs, *Eur. Polym. J.*, 2018, **99**, 259–267.

9 Q. Wu, G. Zhang, M. Gao, L. Huang, L. Li, S. Liu, C. Xie, Y. Zhang and S. Yu, N-doped porous carbon from different nitrogen sources for high-performance supercapacitors and $CO_2$ adsorption, *J. Alloys Compd.*, 2019, **786**, 826–838.

10 H. Sun, Y. Qin, X. Liu and H. Li, Natural Mesoporous Activated Carbon from Toxic Plant Stellera Chamaejasme Roots by Chemical Methods, *J. Bioresour. Bioprod.*, 2018, **3**(2), 84–87.

11 H. Luo, C. C. Zhu, Z. C. Tan, L. W. Bao, J. J. Wang, G. Miao, L. Z. Kong and Y. H. Sun, Preparation of N-doped activated carbons with high $CO_2$ capture performance from microalgae (Chlorococcum sp.), *RSC Adv.*, 2016, **6**(45), 38724–38730.

12 S. M. Hong, S. H. Kim, B. G. Jeong, S. M. Jo and K. B. Lee, Development of porous carbon nanofibers from electrospun polyvinylidene fluoride for $CO_2$ capture, *RSC Adv.*, 2014, **4**(103), 58956–58963.

13 L. Y. Meng and S. J. Park, Effect of heat treatment on $CO_2$ adsorption of KOH-activated graphite nanofibers, *J. Colloid Interface Sci.*, 2010, **352**(2), 498–503.

14 S. Zohdi, M. Anbia and S. Salehi, Improved $CO_2$ adsorption capacity and $CO_2/CH_4$ and $CO_2/N_2$ selectivity in novel hollow silica particles by modification with multi-walled carbon nanotubes containing amine groups, *Polyhedron*, 2019, **166**, 175–185.

15 F. Su, C. Lu, W. Cnen, H. Bai and J. F. Hwang, Capture of $CO_2$ from flue gas *via* multiwalled carbon nanotubes, *Sci. Total Environ.*, 2009, **407**(8), 3017–3023.

16 Y. Zhao, L. Zhao, K. X. Yao, Y. Yang, Q. Zhang and Y. Han, Novel porous carbon materials with ultrahigh nitrogen contents for selective $CO_2$ capture, *J. Mater. Chem.*, 2012, **22**(37), 19726–19731.

17 Z. Liu, Z. Du, W. Xing and Z. Yan, Facial synthesis of N-doped microporous carbon derived from urea furfural resin with high $CO_2$ capture capacity, *Mater. Lett.*, 2014, **117**, 273–275.

18 M. Sevilla, P. Valle-Vigón and A. B. Fuertes, N-doped polypyrrole-based porous carbons for $CO_2$ capture, *Adv. Funct. Mater.*, 2011, **21**(14), 2781–2787.

19 G. Sethia and A. Sayari, Comprehensive study of ultra-microporous nitrogen-doped activated carbon for $CO_2$ capture, *Carbon*, 2015, **93**, 68–80.

20 C. Pevida, T. C. Drage and C. E. Snape, Silica-templated melamine–formaldehyde resin derived adsorbents for $CO_2$ capture, *Carbon*, 2008, **46**(11), 1464–1474.

21 J. Kou and L. B. Sun, Fabrication of nitrogen-doped porous carbons for highly efficient $CO_2$ capture: rational choice of a polymer precursor, *J. Mater. Chem. A*, 2016, **4**(44), 17299–17307.

22 J. Wang, R. Krishna, T. Yang and S. Deng, Nitrogen-rich microporous carbons for highly selective separation of light hydrocarbons, *J. Mater. Chem. A*, 2016, **4**(36), 13957–13966.

23 M. Yang, L. Guo, G. Hu, X. Hu, L. Xu, J. Chen, W. Dai and M. Fan, Highly cost-effective nitrogen-doped porous coconut shell-based $CO_2$ sorbent synthesized by combining ammoxidation with KOH activation, *Environ. Sci. Technol.*, 2015, **49**(11), 7063–7070.

24 E. M. Kutorglo, F. Hassouna, A. Beltzung, D. Kopecký, I. Sedlářová and M. Šoóš, Nitrogen-rich hierarchically porous polyaniline-based adsorbents for carbon dioxide ($CO_2$) capture, *Chem. Eng. J.*, 2019, **360**, 1199–1212.

25 P. Zhang, Y. Zhong, J. Ding, J. Wang, M. Xu, Q. Deng, Z. Zeng and S. Deng, A new choice of polymer precursor for solvent-free method: Preparation of N-enriched porous carbons for highly selective $CO_2$ capture, *Chem. Eng. J.*, 2019, **355**, 963–973.

26 M. Ovcharov, N. Shcherban, S. Filonenko, A. Mishura, M. Skoryk, V. Shvalagin and V. Granchak, Hard template synthesis of porous carbon nitride materials with improved efficiency for photocatalytic $CO_2$ utilization, *Mater. Sci. Eng., B*, 2015, **202**, 1–7.

27 T. N. Phan, M. K. Gong, R. Thangavel, Y. S. Lee and C. H. Ko, Enhanced electrochemical performance for EDLC using ordered mesoporous carbons (CMK-3 and CMK-8): Role of mesopores and mesopore structures, *J. Alloys Compd.*, 2019, **780**, 90–97.

28 L. Sui, Y. Wang, W. Ji, H. Kang, L. Dong and L. Yu, N-doped ordered mesoporous carbon/graphene composites with supercapacitor performances fabricated by evaporation induced self-assembly, *Int. J. Hydrogen Energy*, 2017, **42**(50), 29820–29829.

29 J. Wei, D. Zhou, Z. Sun, Y. Deng, Y. Xia and D. Zhao, A controllable synthesis of rich nitrogen-doped ordered mesoporous carbon for $CO_2$ capture and supercapacitors, *Adv. Funct. Mater.*, 2013, **23**(18), 2322–2328.

30 S. E. Elaigwu and G. M. Greenway, Biomass derived mesoporous carbon monoliths *via* an evaporation-induced self-assembly, *Mater. Lett.*, 2014, **115**, 117–120.

31 S. Kubo, R. J. White, N. Yoshizawa, M. Antonietti and M. M. Titirici, Ordered carbohydrate-derived porous carbons, *Chem. Mater.*, 2011, **23**(22), 4882–4885.

32 S. Feng, W. Li, J. Wang, Y. Song, A. A. Elzatahry and Y. Xia, Hydrothermal synthesis of ordered mesoporous carbons from a biomass-derived precursor for electrochemical capacitors, *Nanoscale*, 2014, **6**(24), 14657–14661.

33 D. Liu, C. Zeng, D. Qu, H. Tang, Y. Li, B. L. Su and D. Qu, Highly efficient synthesis of ordered nitrogen-doped mesoporous carbons with tunable properties and its application in high performance supercapacitors, *J. Power Sources*, 2016, **321**, 143–154.

34 G. P. Hao, W. C. Li, S. Wang, G. H. Wang, L. Qi and A. H. Lu, Lysine-assisted rapid synthesis of crack-free hierarchical

carbon monoliths with a hexagonal array of mesopores, *Carbon*, 2011, **49**(12), 3762–3772.

35 D. Liu, J. H. Lei, L. P. Guo and K. J. Deng, Simple hydrothermal synthesis of ordered mesoporous carbons from resorcinol and hexamine, *Carbon*, 2011, **49**(6), 2113–2119.

36 A. Simaioforidou, V. Kostas, M. A. Karakassides and M. Louloudi, Surface chemical modification of macroporous and mesoporous carbon materials: Effect on their textural and catalytic properties, *Microporous Mesoporous Mater.*, 2019, **279**, 334–344.

37 X. Fu, S. Liu, D. Zhu, Y. Xu and X. Yan, A facile and novel route for the direct synthesis superparamagnetic ordered mesoporous carbon, *Mater. Lett.*, 2019, **234**, 269–271.

38 D. H. Lin, Y. X. Jiang, S. R. Chen, S. P. Chen and S. G. Sun, Preparation of Pt nanoparticles supported on ordered mesoporous carbon FDU-15 for electrocatalytic oxidation of CO and methanol, *Electrochim. Acta*, 2012, **67**, 127–132.

39 Y. Wu, J. Wang, Y. Muhammad, S. Subhan, Y. Zhang, Y. Ling, J. Li, Z. Zhao and Z. Zhao, Pyrrolic N-enriched carbon fabricated from dopamine-melamine *via* fast mechanochemical copolymerization for highly selective separation of $CO_2$ from $CO_2/N_2$, *Chem. Eng. J.*, 2018, **349**, 92–100.

40 A. Rehman and S. J. Park, Comparative study of activation methods to design nitrogen-doped ultra-microporous carbons as efficient contenders for $CO_2$ capture, *Chem. Eng. J.*, 2018, **352**, 539–548.

41 Z. Wu, P. A. Webley and D. Zhao, Post-enrichment of nitrogen in soft-templated ordered mesoporous carbon materials for highly efficient phenol removal and $CO_2$ capture, *J. Mater. Chem.*, 2012, **22**(22), 11379–11389.

42 D. Tiwari, C. Goel, H. Bhunia and P. K. Bajpai, Melamine-formaldehyde derived porous carbons for adsorption of $CO_2$ capture, *J. Environ. Manage.*, 2017, **197**, 415–427.

43 D. Tiwari, H. Bhunia and P. K. Bajpai, Adsorption of $CO_2$ on KOH activated, N-enriched carbon derived from urea formaldehyde resin: kinetics, isotherm and thermodynamic studies, *Appl. Surf. Sci.*, 2018, **439**, 760–771.

44 G. A. Ferrero, A. B. Fuertes, M. Sevilla and M. M. Titirici, Efficient metal-free N-doped mesoporous carbon catalysts for ORR by a template-free approach, *Carbon*, 2016, **106**, 179–187.

45 L. An, S. Liu, L. Wang, J. Wu, Z. Wu, C. Ma, Q. Yu and X. Hu, Novel Nitrogen-Doped Porous Carbons Derived from Graphene for Effective $CO_2$ Capture, *Ind. Eng. Chem. Res.*, 2019, **58**(8), 3349–3358.

46 M. Vorokhta, J. Morávková, D. Řimnáčová, R. Pilař, A. Zhigunov, M. Švábová and P. Sazama, $CO_2$ capture using three-dimensionally ordered micromesoporous carbon, *J. $CO_2$ Util.*, 2019, **31**, 124–134.

47 M. Yuan, G. Gao, X. Hu, X. Luo, Y. Huang, B. Jin and Z. Liang, Premodified Sepiolite Functionalized with Triethylenetetramine as an Effective and Inexpensive Adsorbent for $CO_2$ Capture, *Ind. Eng. Chem. Res.*, 2018, **57**(18), 6189–6200.

48 J. Singh, S. Basu and H. Bhunia, $CO_2$ capture by modified porous carbon adsorbents: Effect of various activating agents, *J. Taiwan Inst. Chem. Eng.*, 2019, **31**, 124–134.

49 S. Divekar, A. Nanoti, S. Dasgupta, Aarti, R. Chauhan, P. Gupta, M. O. Garg, S. P. Singh and I. M. Mishra, Adsorption equilibria of propylene and propane on zeolites and prediction of their binary adsorption with the ideal adsorbed solution theory, *J. Chem. Eng. Data*, 2016, **61**(7), 2629–2637.

50 S. J. Caldwell, B. Al-Duri, N. Sun, C. Sun, H. Liu, C. E. Snape, K. Li and J. Wood, Carbon dioxide separation from nitrogen/hydrogen mixtures over activated carbon beads: adsorption isotherms and breakthrough studies, *Energy Fuels*, 2015, **29**(6), 3796–3807.

51 C. Goel, D. Tiwari, H. Bhunia and P. K. Bajpai, Pure and Binary Gas Adsorption Equilibrium for $CO_2$-$N_2$ on Oxygen Enriched Nanostructured Carbon Adsorbents, *Energy Fuels*, 2017, **31**(12), 13991–13998.

52 C. Chen, H. Huang, Y. Yu, J. Shi, C. He, R. Albilali and H. Pan, Template-free synthesis of hierarchical porous carbon with controlled morphology for $CO_2$ efficient capture, *Chem. Eng. J.*, 2018, **353**, 584–594.

53 J. Xu, J. Shi, H. Cui, N. Yan and Y. Liu, Preparation of nitrogen doped carbon from tree leaves as efficient $CO_2$ adsorbent, *Chem. Phys. Lett.*, 2018, **711**, 107–112.

54 L. Yue, Q. Xia, L. Wang, L. Wang, H. DaCosta, J. Yang and X. Hu, $CO_2$ adsorption at nitrogen-doped carbons prepared by $K_2CO_3$ activation of urea-modified coconut shell, *J. Colloid Interface Sci.*, 2018, **511**, 259–267.

55 W. Xing, C. Liu, Z. Zhou, L. Zhang, J. Zhou, S. Zhuo, Z. Yan, H. Gao, G. Wang and S. Z. Qiao, Superior $CO_2$ uptake of N-doped activated carbon through hydrogen-bonding interaction, *Energy Environ. Sci.*, 2012, **5**(6), 7323–7327.

56 A. L. Myers and J. M. Prausnitz, Thermodynamics of mixed gas adsorption, *AIChE J.*, 1965, **11**(1), 121–127.

57 R. Krishna, S. Calero and B. Smit, Investigation of entropy effects during sorption of mixtures of alkanes in MFI zeolite, *Chem. Eng. J.*, 2002, **88**(1–3), 81–94.

58 Z. Zhang, S. Xian, Q. Xia, H. Wang, Z. Li and J. Li, Enhancement of $CO_2$ adsorption and $CO_2/N_2$ selectivity on ZIF-8 *via* postsynthetic modification, *AIChE J.*, 2013, **59**(6), 2195–2206.

59 X. Ma, L. Li, Z. Zeng, R. Chen, C. Wang, K. Zhou and H. Li, Experimental and theoretical demonstration of the relative effects of O-doping and N-doping in porous carbons for $CO_2$ capture, *Appl. Surf. Sci.*, 2019, **481**, 1139–1147.

60 L. Rao, R. Ma, S. Liu, L. Wang, Z. Wu, J. Yang and X. Hu, Nitrogen enriched porous carbons from d-glucose with excellent $CO_2$ capture performance, *Chem. Eng. J.*, 2019, **362**, 794–801.

61 L. Yue, L. Rao, L. Wang, L. An, C. Hou, C. Ma, H. DaCosta and X. Hu, Efficient $CO_2$ adsorption on nitrogen-doped porous carbons derived from d-glucose, *Energy Fuels*, 2018, **32**(6), 6955–6963.

62 L. Rao, S. Liu, L. Wang, C. Ma, J. Wu, L. An and X. Hu, N-doped porous carbons from low-temperature and single-step sodium amide activation of carbonized water chestnut shell with excellent $CO_2$ capture performance, *Chem. Eng. J.*, 2019, **359**, 428–435.